Editors' Suggestion

Role of geometry and adhesion in droplet freezing dynamics

Lila Seguy and Suzie Protiere
Institut Jean le Rond d'Alembert, Sorbonne Université, CNRS UMR 7190, F-75005 Paris, France

Axel Huerre
MSC, Université Paris Cité, CNRS UMR 7057, F-75013 Paris, France

(Received 30 September 2022; accepted 24 January 2023; published 9 March 2023)

We study the freezing of water drops on a copper substrate for temperatures ranging from −9 to −79 °C. We propose a thermal and geometrical analytical model for the freezing front dynamics. It assumes a propagation of the front at the center described by the three-phase (liquid, ice, substrate) Stefan model in one dimension. The growth is characterized by an effective diffusion coefficient that increases as the substrate temperature decreases. We also consider a spherical front that meets the edges of the drop perpendicularly. Our model captures well our experimental data between −9 and −40 °C and highlights the importance of the heat diffusion in the liquid for the freezing process. Beyond these temperatures, the adhesion of the drops to the copper decreases and the substrate temperature must be considered equal to −41 °C to rationalize the experimental findings.

DOI: 10.1103/PhysRevFluids.8.033601

I. INTRODUCTION

From a fundamental point of view, a droplet is the most obvious object to study heat transfer in a spherical geometry. The solidification of a drop is a complex phenomenon described by several phases. The droplet is either deposited on a substrate that is cooled down afterwards or is brought in contact with the subcooled surface. It then spreads and stops at a given radius with a well-defined contact angle θ [1]. A front of ice forms and grows vertically in the water. As the ice replaces water, the droplet's shape is affected and ultimately a pointy tip is observed at the apex. This peculiar shape drew attention from the early comment of Stairs [2] to the more advanced descriptions of the phenomenon [3–9].

The freezing of water droplets on a cold substrate is also commonly observed in industry, especially for aircraft [10] and wind turbines [11], where the presence of frozen droplets can reduce their performance or interfere with the measurement devices, with sometimes dramatic consequences. A commonly derived feature is the solidification time (the time it takes for the drop to be totally solidified) as technical solutions will involve timescales that must be compared to this time. It was shown for example that it decreases when the temperature difference between the substrate and the freezing temperature increases. This solidification time results from the dynamics of the solidification front over time. However, due to the complex nature of the problem (geometry [12], phase change, volume change, and the presence of the substrate [13,14] and of dissolved gases [15]), very few studies report the dynamics of the solidification front in droplets.

In this paper, we perform a large set of experiments of water droplet solidification, varying the temperature of the substrate from −9 to −79 °C. We record the position of the solidification front within the droplet and build an analytical model to reproduce our experimental data. Finally,

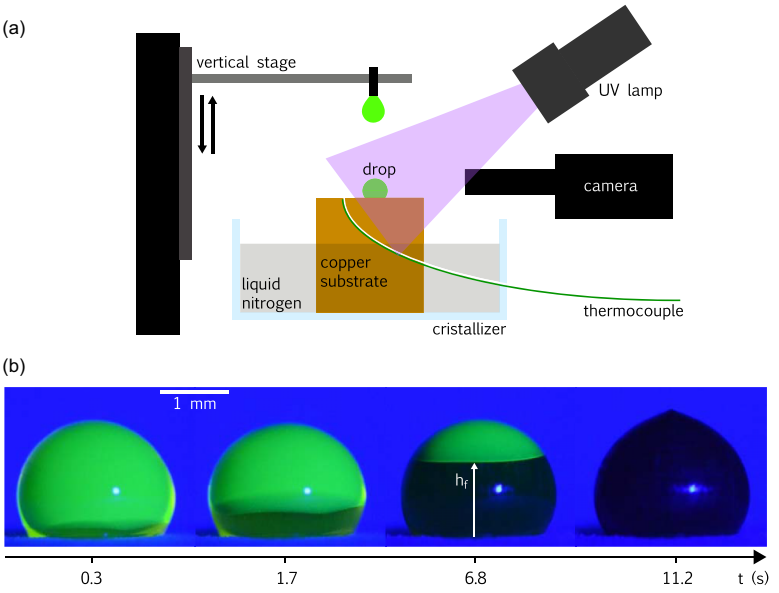

FIG. 1. (a) Experimental setup. A drop is deposited with a motorized vertical translation stage on a copper cylinder of diameter $D = 10$ cm. The substrate is cooled in liquid nitrogen and its temperature is measured over time. A drop of controlled volume $V = 7$ or 13 μL is generated using a syringe pump. The drop is composed of a mixture of 0.5 g/L fluorescein and water. A UV lamp is placed to reveal the fluorescence. A Nikon D850 camera equipped with a 12× objective is used to film the freezing process over time, with a frame rate of 60 frames/s. (b) Typical experiment showing the freezing front dynamics for $T_s = -40.9\,^\circ$C and $V = 13$ μL. (See Supplemental Movie 1 [16].)

we highlight the importance of adhesion once the drop is placed in contact with the substrate to understand our experimental results below $-40\,^\circ$C.

II. EXPERIMENTAL SETUP

We place a droplet of pure de-ionized water (Merck Millipore Type II) on a cylindrical copper substrate with a diameter and height 10 cm, and a thermal conductivity of $k_s = 398$ W m^{-1} K^{-1}. We use a Thorlabs vertical translation stage mounted with a stepped motor in order to control the drop's deposition: A hanging drop of known volume ($V = 7$ or 13 μL) is formed at the tip of a needle of diameter 0.41 mm; at a specific distance, the translation stage brings the drop in contact with the substrate and immediately retracts at the velocity of 30 mm s^{-1} [Fig. 1(a)]. Fluorescein is added to the water droplet (concentration 0.5 g L^{-1}). Since the ice rejects fluorescein molecules or captures highly concentrated clusters, the frozen portion of the drop has a low concentration of fluorescein and thus does not fluoresce when a UV light is shone on the drop [17]. This experimental technique enables us to precisely visualize the freezing front [Fig. 1(b)].

To cool the copper substrate to the desired temperature, we place it in a crystallizer filled with liquid nitrogen. We let the liquid nitrogen evaporate, thus the substrate is homogeneously cooled down at a very low temperature and will slowly go back to ambient temperature ($\approx$0.5 $^\circ$C min^{-1}). The temperature is then continuously monitored using thermocouples placed on the cylinder's surface. The dimensions of the copper block enable us to keep a constant substrate temperature during the whole freezing process (variation lower than 1 $^\circ$C), which ranges between 10 and 40 s. When working at temperatures close to $T_f = 0\,^\circ$C, the freezing process lasts longer than 20 s, and we then use a Julabo 1000F thermostatic bath to keep the substrate temperature variation around 0.1 $^\circ$C.

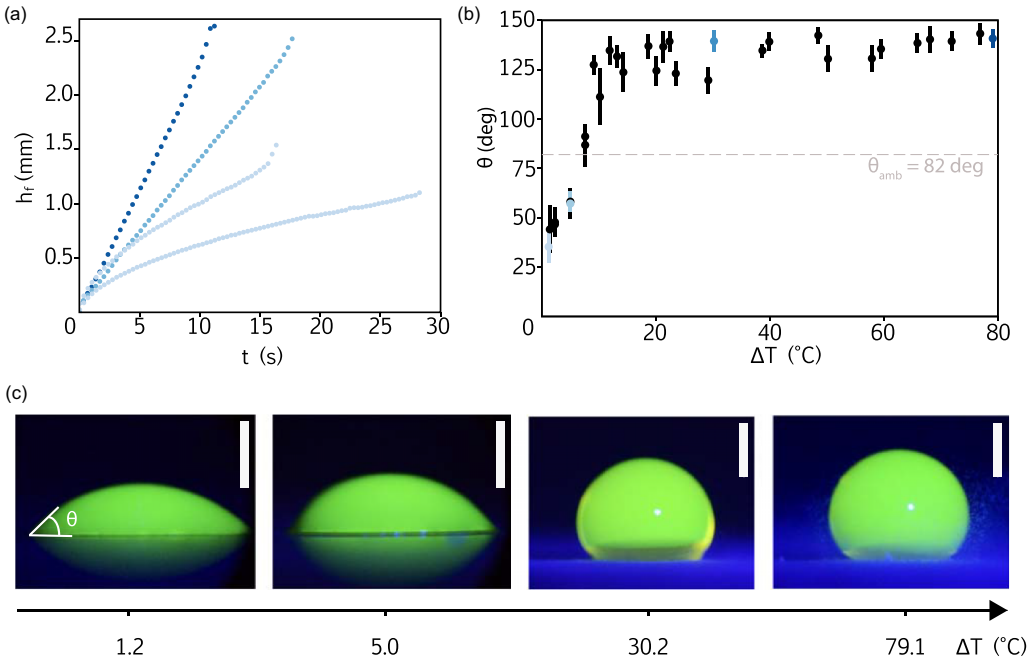

FIG. 2. (a) Front height h_f (mm) vs time t (s) for different temperatures (from lighter blue to darker blue) $(T_s, V) = [(-1.2, 7), (-5.0, 7), (-30.2, 13), (-79.1, 13)]$ (°C, μL). (b) The contact angle θ vs ΔT. Blue points correspond to the experiments presented in (a). The dashed gray line represents the contact angle at ambient temperature. (c) Snapshots of drops at different substrate temperatures and volumes $(T_s, V) = [(-1.2, 7), (-5.0, 7), (-30.2, 13), (-79.1, 13)]$ (°C, μL) corresponding to freezing fronts presented in (a). The scale bar represents 1 mm.

The range of tested substrate temperatures is from $T_s = -80\,°C$ to $T_s = -1\,°C$. The temperature of the drop is measured using a thermocouple inserted in the upper part of the syringe depositing the drop and is about 20 °C. Its precise value is reported for each experiment. Before depositing the drop, frost is removed from the substrate with a spatula and a tissue as it can both interfere with the visualization of the front and the freezing dynamics [8]. The freezing process is filmed at a frequency of 60 frames/s with a Nikon D850 camera and a Navitar 12× objective. Typical images of the freezing front dynamics are presented in Fig. 1(b). The freezing front at the edge of a drop $h_f(t)$ is then measured by image analysis.

III. RESULTS

We measure the freezing front $h_f(t)$ as a function of time for different temperatures ranging between $1\,°C < \Delta T = T_f - T_s < 80\,°C$ [Fig. 2(a)]. We observe two different freezing front dynamics. At low ΔT ($\Delta T = 1.2\,°C$ and $\Delta T = 5\,°C$), we find that at first the freezing front increases rapidly and then slows down similarly to a square-root function (light blue points), which corresponds to a phenomenon intensely investigated experimentally [7,13,18] and numerically [13,19–21]. At higher values of ΔT ($\Delta T = 30.2$ and $79.1\,°C$), however, the freezing front seems to grow linearly (dark blue points). If we look closely at the shape of the drop after placing it on the substrate at these different temperatures, we find that its shape varies greatly [Fig. 2(c)]. Indeed, at low ΔT, the drop looks hemispherical with a contact angle $\theta < 90°$, whereas at higher ΔT, the shape of the drop is almost spherical with $\theta > 90°$. We measure the contact angle θ for different temperatures in Fig. 2(b). At $\Delta T = 0\,°C$, θ is close to 40°. It then increases sharply up to a critical value

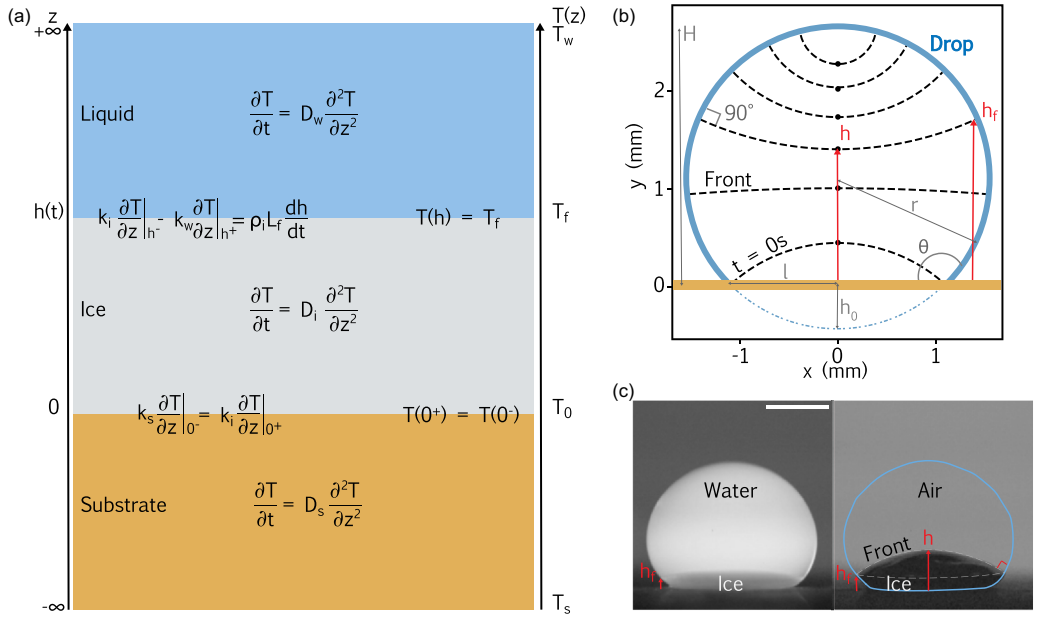

FIG. 3. (a) Diagram of the Stefan 1D problem with a semi-infinite substrate and liquid domains and diffusion taken into account everywhere. (b) Theoretical front (dashed line) in the central plane of the spherical drop (in blue) at different times. (c) Snapshots of a drop just before (left) and after (right) being interrupted during its freezing. The upper liquid part has been removed so as to show the shape of the freezing front (right picture).

$\Delta T_I^* \approx 10\,^\circ$C where it remains constant and close to $\theta = 130^\circ$. This change in contact angle can be explained by a competition between wetting and freezing of the contact line at the time of drop deposition [1,22,23]. The observed contact angle is the result of an imposed contact area on a spherical interface. Indeed, the larger ΔT is, the more the freezing speed increases and pins the drop at a contact angle higher than the wetting angle on the copper at room temperature. A cold substrate leads to the formation of a droplet of similar shape to the one that could be observed on a hydrophobic surface.

To build a model to explain the freezing front dynamics, we fix our temperature range of interest at $\Delta T > 10\,^\circ$C, as we focus on the freezing front dynamics of spherical drops. This choice is justified as, in this range of temperature, the contact angle remains roughly constant and thus the drop shape remains similar above this critical value. Moreover, a geometrical model has already been developed for hemispherical drops [6].

IV. THEORETICAL MODEL

In order to build a simple analytical model to understand the dynamics of the front at the drop edges (the front position we are able to measure), we first use the one-dimensional (1D) semi-infinite domain Stefan problem with diffusion in water to model the growth of the freezing front at the center of the drop [schematized in Fig. 3(a)]. Regarding the thermal conductivity of the air ($0.026\ \mathrm{W\,m^{-1}\,K^{-1}}$ at $25\,^\circ$C), it seems legitimate to consider the vertical boundaries of our system as adiabatic. We then assume a spherical freezing front and impose a third condition: the orthogonal connection between the front and the edges of the drop. We can thus define the radius of curvature of the front. Those last two assumptions are supported by previous studies [5,20] and confirmed by our own experimental observations. Indeed, when we interrupt the freezing of a drop by wiping

away the remaining water at different times we can observe the shape of the front and find that it forms a spherical cap that is connected perpendicularly to the edges [Fig. 3(c)]. This particular shape of the freezing front is conditioned by the contact angle of the drop. In the case of a drop with a contact angle below 90°, the shape of the front is not exactly a portion of a sphere, as the presence of the substrate will perturb the sphericity of the front. In the experiments we consider for the model, $\theta > 90°$, and consequently the freezing front is initially oriented towards the top of the drop, avoiding the influence of the substrate on the freezing front shape.

Finally, the 1D space is separated into three domains: For z going from $-\infty$ to 0 we have the substrate, for z going from 0 to $h(t)$ the ice, and from $h(t)$ to $+\infty$ the liquid. Each domain diffuses heat according to its respective diffusion coefficient. The substrate is at temperature T_s for $z \to -\infty$ and the liquid at temperature T_w for $z \to +\infty$. The properties of the materials lead to a certain contact temperature T_0 at the ice/substrate interface ($z = 0$), which is higher than T_s and depends on the thermal properties of the substrate. The precise dependence of T_0 as a function of ΔT and T_w is plotted in the Supplemental Material [Fig. 1(c)] [16]. The freezing front is at temperature $T_f = 0\,°\mathrm{C}$. At $z = 0$ we assume equal heat fluxes and the Stefan condition on the fluxes is set at $z = h(t)$. We then obtain a self-similar solution of the height of the front:

$$h(t) = 2\alpha\sqrt{D_i t}. \tag{1}$$

The freezing front evolves as a square root of time with a diffusion coefficient $\alpha^2 D_i$, with α satisfying the transcendental equation

$$\frac{\mathrm{St_i}}{\frac{e_i}{e_s} + \mathrm{erf}(\alpha)} e^{-\alpha^2} - \frac{\gamma\sqrt{\beta}\,\mathrm{St_w}}{\mathrm{erf}(\alpha/\sqrt{\beta}) - 1} e^{-\alpha^2\beta} = \alpha\sqrt{\pi}, \tag{2}$$

with $e_i = \sqrt{\rho_i k_i c_{p,i}}$ and e_s being respectively the ice and substrate effusivities which characterize the ability of a material to have a contact temperature close to its temperature ($e_s = 36\,490\ \mathrm{W\,m^{-2}\,K^{-1}\,s^{-1/2}}$ for copper and $e_i = 2031\ \mathrm{W\,m^{-2}\,K^{-1}\,s^{-1/2}}$ for ice). $\mathrm{St_i} = \frac{(T_f - T_s)c_{p,i}}{L_f}$ is the Stefan number of the ice, L_f the enthalpy of fusion, $c_{p,i}$ the specific heat capacity of ice, $\mathrm{St_w} = \frac{(T_f - T_w)c_{p,w}}{L_f}$ a similar Stefan number for the liquid, $\beta = \frac{D_i}{D_w}$ the ratio of diffusion coefficients of the ice and the liquid, $\gamma = \frac{\rho_w}{\rho_i}$ the ratio of densities, and $k_{i,s}$ the heat conductivities of the ice and substrate, respectively [13,14]. Here, the second term, related to the heat diffusion in the liquid phase, decreases the value of α for higher liquid temperatures T_w: The diffusion in the liquid part slows down the ascent of the freezing front [see the surface map of $\alpha(T_s, T_w)$ in Fig. 1 in the Supplemental Material [16]].

Moreover, the diffusion from the warm liquid part causes a critical substrate temperature T_{crit} for which the interface temperature T_0 is above 0 °C, as $T_0 > T_s$. We note that this implies that freezing is theoretically impossible for temperatures higher than T_{crit}. With our experimental parameters, $T_{crit} = -0.87\,°\mathrm{C}$, which is well above $\Delta T_l^* \approx 10\,°\mathrm{C}$, the starting temperature of our range of study.

When the drop is spherical, the front meets the edge of the drop at 90°, ensuring the nullity of the thermal fluxes in the air [Fig. 3(c) and 2D experiments [5]]. We therefore assume a spherical freezing front that is at a height $h(t)$ at the center of the drop and perpendicularly connects at a height $h_f(t)$ with the drop's edge [Fig. 3(b)]. For $\theta = 180°$, the drop is a sphere and $h_{f,\mathrm{sphere}}(t)$ can be determined with geometrical considerations,

$$h_{f,\mathrm{sphere}}(t) = r\left\{1 - \cos\left[-2\arctan\left(\frac{2\alpha\sqrt{D_i t}}{2\alpha\sqrt{D_i t} - 2r}\right)\right]\right\}, \tag{3}$$

with r being the drop's radius. However, the drop is a portion of the sphere, and as such it has a contact disk with the substrate of radius l. We subtract to the height $h_0 = r - \sqrt{r^2 - l^2}$, the difference of height between the full sphere and a portion of the sphere [see schematics in Fig. 3(b)]. The time is reset to t_0, the time it takes to reach a height h_0 in a full sphere geometry: $h_{f,\mathrm{sphere}}(t_0) = h_0$. Thus, the front at the center is not at $h = 0$ for $t = 0$, as seen in Fig. 3(b). This

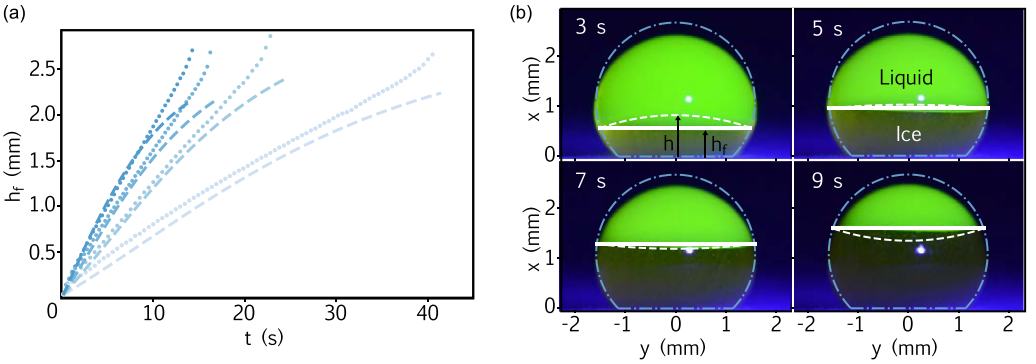

FIG. 4. (a) Theoretical fronts (dashed lines) and experimental fronts (dots) $h_f(t)$ for $\Delta T = 11.9, 23.5, 29.2, 38.7\,^\circ$C (from light to dark blue). (b) Overlay of theoretical drop profile (blue line) and freezing front at the edges (white line) and at the center (dotted white line) of a spherical drop for different times at $\Delta T = 38.7\,^\circ$C. The experimental front corresponds to the interface between the liquid part which fluoresces green and the dark solid part which no longer contains fluorescein.

is equivalent to physically assuming that the front grows by a certain height inside the drop before reaching the edges [24,25]. Finally, we can express the height of the solidification front at the edges of the drop,

$$h_f(t) = r\left\{1 - \cos\left[-2\arctan\left(\frac{2\alpha\sqrt{D_i(t+t_0)}}{2\alpha\sqrt{D_i(t+t_0)} - 2r}\right)\right]\right\} - r\left[1 - \sqrt{1 - \left(\frac{l}{r}\right)^2}\right], \tag{4}$$

with

$$t_0 = \frac{1}{4\alpha^2 D_i}\left(\frac{2r\tan\left[-\frac{1}{2}\arccos\sqrt{1-(l/r)^2}\right]}{\tan\left[-\frac{1}{2}\arccos\sqrt{1-(l/r)^2}\right] - 1}\right)^2. \tag{5}$$

We observe that Eq. (4) now also depends on the contact surface with the substrate of radius l. In the particular case of the sphere, $l = 0$, and we find the expression $h_{f,\mathrm{sphere}}(t)$, as the second term of Eq. (4) is canceled and $t_0 = 0$.

We compare this theoretical model [Eq. (4)] to our experimental results [Fig. 4(a)] for ΔT between 10 and 40 °C and find a good agreement without the use of any prefactor. This agreement highlights the importance of taking into account the diffusion in the liquid portion and validates the model's hypotheses. Noticeably, the theoretical curves do not follow the experimental curves when the freezing front is close to the top of the droplet and several reasons could explain this observation. Indeed, the volume change linked to the water-ice phase change is not taken into account in the model and is responsible for the creation of a pointy tip [6], visible in the last stage of the front dynamics. We also assumed a one-dimensional Stefan problem at the center which could break in the later stage of freezing. At that point, the drastic change in cross section with the height could allow lateral heat fluxes to develop, allowing for a faster cooling than the model prediction. Theoretical freezing front profiles are also compared to a typical experiment at different times [Fig. 4(b)]. We observe that the circle fitting the drop is less relevant at its top and that the real section of the drop is thinner than the theoretical one, which could also explain the faster experimental freezing dynamics observed in the final stage.

The model proposed here may thus be improved by adapting the diffusion coefficient at the drop's center to this change in cross section. The addition of such assumptions to the current Stefan model would however disturb the self-similarity of the solution.

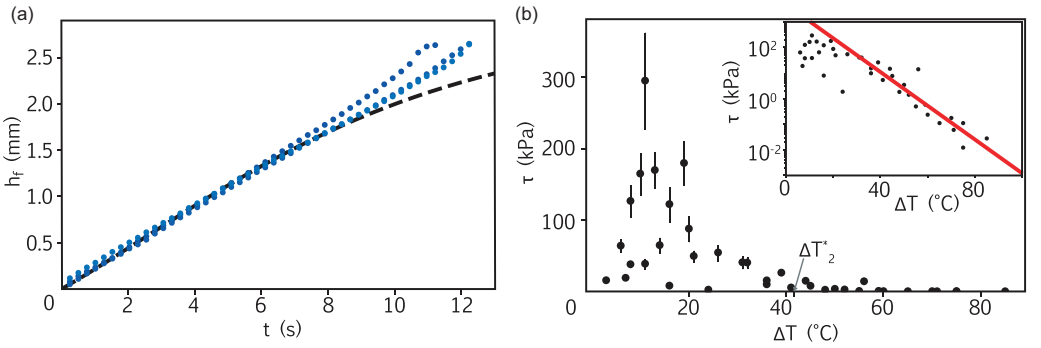

FIG. 5. (a) Experimental front $h_f(t)$ for $\Delta T = (50.2, 59.5, 79.1)\,^\circ$C (blue points) and theoretical front for a spherical drop with $T_s = -41\,^\circ$C (dashed line). (b) Adhesion of a water droplet to the copper substrate τ as a function of ΔT. Log-linear plot in the inset showing an exponential decrease.

Finally, for $\Delta T = 11.9\,^\circ$C, the theoretical curve is much slower than the experimental one and should be adapted. The assumption of a semi-infinite liquid medium shows its limit here. It remains valid as long as the thermal boundary layer of thickness $\delta = \sqrt{D_w \tau_{freeze}}$ is smaller than the drop's height H. This leads to $\tau_{freeze} < 40$ s, a condition that is found experimentally for $\Delta T > \Delta T_1^* = 10\,^\circ$C. Below this temperature, the temperature of the water should be considered lower, leading to a faster solidification front, as observed in the experiment in light blue in Fig. 4(a). Nevertheless, our model matches well the freezing front's dynamics for higher ΔT, during most of the duration of the experiment.

V. ADHESION TO THE SUBSTRATE

For cold substrates with $\Delta T > \Delta T_2^* = 40\,^\circ$C the freezing front dynamics becomes independent of the substrate temperature [Fig. 5(a)]. Moreover, the behavior of the freezing front can be adjusted with our model if considering a substrate temperature of $T_s = -41\,^\circ$C [dashed line in Fig. 5(a)]. For such high values of ΔT, the freezing considered is thus much slower than expected. We hypothesize that the adhesion of the ice on the substrate plays an important role here. Indeed, in those experiments, we observe that depending on the temperature, the drop seemed to adhere differently on the substrate.

After placing a drop on the copper substrate using the same experimental setup described in the previous section, we use a force sensor Futek IPM650 to apply a horizontal force F on the drop until it detaches from the substrate in order to measure its adhesion. The experiment was performed for ΔT ranging from 0 to 90 °C. We were able to measure A, the contact area of the drop on the ice, by image analysis and found τ, the adhesion of the water droplet on ice:

$$\tau = \frac{F}{A}. \tag{6}$$

We can then characterize the adhesion of the ice as a function of ΔT [Fig. 5(b)]. As our sensor is not exactly located at the base of the drop, a torque is added and we possibly obtain slightly higher values than in reality. However, our measurements are within the same experimental range as the ones measured using a similar technique and materials [26]. We must note however that various methods exist to measure the adhesion of water on ice and lead to extremely different values [27] as frost, contact angle, substrate roughness, or dissolved gas in water may affect the measurements [28,29]. We can nevertheless observe an exponential decrease of τ beyond $\Delta T \approx 10\,^\circ$C. We also measure the critical temperature ΔT_2^* beyond which the drop does not adhere

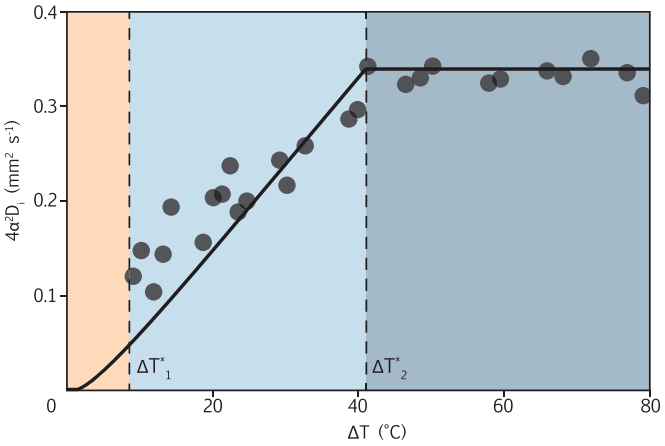

FIG. 6. Experimental (black spheres) and theoretical (black line) $4\alpha^2 D_\mathrm{i}$ vs ΔT. The yellow region corresponds to the wetting drops that we did not study. The light blue zone corresponds to nonwetting drops with $4\alpha^2 D_\mathrm{i}$ increasing with ΔT. The dark blue zone corresponds to the nonwetting drops with constant $4\alpha^2 D_\mathrm{i}$ due to loss of adhesion.

to the substrate by fitting the function $\tau \propto \exp(-T/T_2^*)$ to this curve [inset of Fig. 5(b)]. We find that $\Delta T_2^* \sim 45\,^\circ\mathrm{C}$. Different theories are proposed to explain the adhesion of ice on substrates [30,31]. In particular, Ref. [32] describes the delamination phenomenon: When the substrate's temperature is low, the freezing rate will be high and the lower part of the drop will capture an important amount of air bubbles [33]. The stress in the frozen drop due to thermal contraction will be released by cracks or delamination (self-peeling of the drop) depending on whether or not the ice cohesion is higher than the adhesion to the substrate. The bubble layer at very low temperature reduces the adhesion and favors delamination. This loss in contact area with the substrate slows down the freezing, as the thermal conductivity of air is approximately 10 000 times lower than copper.

For $\Delta T > \Delta T_2^*$, the thermal contact between the drop and the substrate is very poor, limiting the cooling flux. As a consequence, a change in the temperature does not affect the dynamics of the freezing front, as observed in Fig. 5(a) where all the curves are superimposed. It would be interesting to use a poorly conducting substrate instead of copper in order to test whether such critical temperatures are still observed and how they vary.

VI. DISCUSSION

We plot the parameter $4\alpha^2 D_\mathrm{i}$ characterizing the rise of the freezing front at the center of the drop as a function of ΔT (Fig. 6). $4\alpha^2 D_\mathrm{i}$ is obtained by fitting Eq. (4) to the experimental data of the freezing front dynamics at different temperatures (black circles, Fig. 6). The theoretical black line is obtained by solving numerically Eq. (2).

We observe two regions: For $\Delta T > \Delta T_2^* = 41\,^\circ\mathrm{C}$, $4\alpha^2 D_\mathrm{i}$ is measured constant with the temperature. In this region, the data are well described by the theoretical curve considering that the substrate temperature is always $T_\mathrm{s} = -41\,^\circ\mathrm{C}$. For $\Delta T_1^* = 10\,^\circ\mathrm{C} < \Delta T < \Delta T_2^* = 41\,^\circ\mathrm{C}$, the theory describes well the experimental data without any fitting parameters. The agreement between theory and experiments improves as ΔT increases and we notice a slight dispersion of the data points for $\Delta T < 20\,^\circ\mathrm{C}$. It may be due, as detailed earlier, to the decrease of T_w accelerating the rise of the front. This decrease could be due to the presence of the ice itself and also to the presence of evaporation which could become important for longer experiments [8].

VII. CONCLUSION

In this paper, we measured the growth of the freezing front of a water drop of volume $\approx 10\ \mu$L placed on a copper substrate at a temperature between -10 and $-80\,^{\circ}$C so that the contact angle of the droplet remains approximately constant (between 120° and 140°) within this temperature range. The droplet can be considered spherical and we have then established an analytical model for the dynamics of the freezing front based on three assumptions: (i) At the center of the drop, the rise of the front is governed by the semi-infinite one-dimensional three-phase Stefan model, (ii) the front is spherical, and (iii) it connects perpendicularly to the edges of the drop. However, this model does not take into account any possible volume change or the formation of the tip close to the top of the droplet at the end of the freezing dynamics. For temperatures between -20 and $-40\,^{\circ}$C, we observe a good agreement between the model and the experiments without any prefactor. This result shows that the phenomenon of diffusion in water is not negligible and must be taken into account. Below $-40\,^{\circ}$C, the adhesion of the ice to the substrate is poor and an insulating air layer slows down the freezing: The effective diffusion coefficient is found constant. This adhesion force has been measured with a force sensor and gives a critical temperature of adhesion to the substrate around $-40\,^{\circ}$C. Our model still agrees with the data provided that we assume a constant substrate temperature equal to $-41\,^{\circ}$C.

[1] R. Grivet, A. Monier, A. Huerre, C. Josserand, and T. Séon, Contact Line Catch Up by Growing Ice Crystals, Phys. Rev. Lett. **128**, 254501 (2022).

[2] R. A. Stairs, Changes of drop-shapes on freezing, Anal. Chem. **43**, 1535 (1971).

[3] D. M. Anderson, M. Grae Worster, and S. H. Davis, The case for a dynamic contact angle in containerless solidification, J. Cryst. Growth **163**, 329 (1996).

[4] W. W. Schultz, M. G. Worster, and D. M. Anderson, Solidifying sessile water droplets, in *Interactive Dynamics of Convection and Solidification*, edited by P. Ehrhard, D. S. Riley, and P. H. Steen (Springer, Dordrecht, 2001), pp. 209–226.

[5] A. G. Marín, O. R. Enríquez, P. Brunet, P. Colinet, and J. H. Snoeijer, Universality of Tip Singularity Formation in Freezing Water Drops, Phys. Rev. Lett. **113**, 054301 (2014).

[6] M. Nauenberg, Theory and experiments on the ice-water front propagation in droplets freezing on a subzero surface, Eur. J. Phys. **37**, 045102 (2014).

[7] X. Zhang, X. Wu, and J. Min, Freezing and melting of a sessile water droplet on a horizontal cold plate, Exp. Therm. Fluid Sci. **88**, 1 (2017).

[8] J. Sebilleau, E. Ablonet, P. Tordjeman, and D. Legendre, Air humidity effects on water-drop icing, Phys. Rev. E **104**, L032802 (2021).

[9] F. Boulogne and A. Salonen, Drop freezing: Fine detection of contaminants by measuring the tip angle, Appl. Phys. Lett. **116**, 103701 (2020).

[10] G. Poots, R. W. Gent, N. P. Dart, and J. T. Cansdale, Aircraft icing, Philos. Trans. R. Soc. A **358**, 2873 (2000).

[11] G. Fortin and J. Perron, Wind turbine icing and de-icing, in *47th AIAA Aerospace Sciences Meeting including The New Horizons Forum and Aerospace Exposition* (American Institute of Aeronautics and Astronautics, Reston, VA, 2009).

[12] H. F. Zhang, Y. Zhao, R. Lv, and C. Yang, Freezing of sessile water droplet for various contact angles, Int. J. Therm. Sci. **101**, 59 (2016).

[13] M. Stiti, G. Castanet, A. Labergue, and F. Lemoine, Icing of a droplet deposited onto a subcooled surface, Int. J. Heat Mass Transf. **159**, 120116 (2020).

[14] V. Thiévenaz, T. Séon, and C. Josserand, Solidification dynamics of an impacted drop, J. Fluid Mech. **874**, 756 (2019).

[15] Y. Li, M. Li, C. Dang, and X. Liu, Effects of dissolved gas on the nucleation and growth of ice crystals in freezing droplets, Int. J. Heat Mass Transf. **184**, 122334 (2022).

[16] See Supplemental Material at http://link.aps.org/supplemental/10.1103/PhysRevFluids.8.033601 for Fig. S1: Theoretical study of parameter of the transcendental equation and critical substrate temperature with water and substrate temperature. Fig. S2: Influence of water temperature on the dynamics.
[17] D. Dedovets and S. Deville, Multiphase imaging of freezing particle suspensions by confocal microscopy, J. Eur. Ceram. Soc. **38**, 2687 (2018).
[18] X. Zhang, X. Liu, J. Min, and X. Wu, Shape variation and unique tip formation of a sessile water droplet during freezing, Appl. Therm. Eng. **147**, 927 (2019).
[19] Y. Yao, C. Li, H. Zhang, and R. Yang, Modelling the impact, spreading and freezing of a water droplet on horizontal and inclined superhydrophobic cooled surfaces, Appl. Surf. Sci. **419**, 52 (2017).
[20] S. Lyu, K. Wang, Z. Zhang, A. Pedrono, C. Sun, and D. Legendre, A hybrid VOF-IBM method for the simulation of freezing liquid films and freezing drops, J. Comput. Phys. **432**, 110160 (2021).
[21] T. V. Vu, G. Tryggvason, S. Homma, and J. C. Wells, Numerical investigations of drop solidification on a cold plate in the presence of volume change, Int. J. Multiphase Flow **76**, 73 (2015).
[22] V. Thiévenaz, T. Séon, and C. Josserand, Freezing-damped impact of a water drop, Europhys. Lett. **132**, 24002 (2020).
[23] C. A. Knight, The contact angle of water on ice, J. Colloid Interface Sci. **25**, 280 (1967).
[24] C. Gurganus, A. B. Kostinski, and R. A. Shaw, High-speed imaging of freezing drops: Still no preference for the contact line, J. Phys. Chem. C **117**, 6195 (2013).
[25] Y. Ueki, Y. Tsutsumi, and M. Shibahara, Molecular dynamics study of instantaneous interfacial thermal resistance of droplets on flat crystalline surface during cooling and ice formation, Int. J. Heat Mass Transf. **194**, 123004 (2022).
[26] M. E. R. Walford, D. M. Hargreaves, S. Stuart-Smith, and M. Lowson, Freezing of water drops on a cold surface, J. Glaciol. **37**, 47 (1991).
[27] M. Bleszynski and E. Clark, Current ice adhesion testing methods and the need for a standard: A concise review, Standards **1**, 117 (2021).
[28] H. Deng, S. Chang, and W. Li, Experimental study on ice adhesion forces of the copper plates with specific contact angle and roughness, Sustain. Energy Technol. Assess. **43**, 100942 (2021).
[29] A. J. Meuler, J. D. Smith, K. K. Varanasi, J. M. Mabry, G. H. McKinley, and R. E. Cohen, Relationships between water wettability and ice adhesion, ACS Appl. Mater. Interfaces **2**, 3100 (2010).
[30] I. A. Ryzhkin and V. F. Petrenko, Physical mechanisms responsible for ice adhesion, J. Phys. Chem. B **101**, 6267 (1997).
[31] F. Guerin, C. Laforte, M.-I. Farinas, and J. Perron, Analytical model based on experimental data of centrifuge ice adhesion tests with different substrates, Cold Reg. Sci. Technol. **121**, 93 (2016).
[32] D. Song, Y. Jiang, T. Chou, K. Asawa, and C.-H. Choi, Spontaneous deicing on cold surfaces, Langmuir **36**, 11245 (2020).
[33] J. de Ruiter, D. Soto, and K. K. Varanasi, Self-peeling of impacting droplets, Nat. Phys. **14**, 35 (2018).